DOI: 10.1002/ejic.200700060

Red-to-Yellow Pressure-Induced Phase Transition in $Pt(bpy)Cl_2$: Spectroscopic Study Supported by DFT Calculations

Rafael Valiente,*[a] Juan M. García-Lastra,[b] Pablo García-Fernández,[c] Sara García-Revilla,[d] and Oliver S. Wenger[e]

Keywords: Phase transition / High-pressure chemistry / DFT calculations / Platinum(II) / Metal–metal interactions

The combination of spectroscopic and computational methods has been employed to explore the origin of the luminescence in the red and yellow forms of $Pt(bpy)Cl_2$. The luminescence of the red (linear-chain) form of $Pt(bpy)Cl_2$ (bpy = 2,2′-bipyridine) has been measured as a function of hydrostatic pressure up to 65 kbar. The luminescence band maximum is redshifted (–147 $cm^{-1}\,kbar^{-1}$), and the intrachain Pt–Pt distance decreases from 3.46 to 3.25 Å between ambient pressure and 17.7 kbar. Strong discontinuities in the optical properties at 17.7 kbar were interpreted in terms of a crystallographic phase transition from the red to a denser yellow form of $Pt(bpy)Cl_2$. First-principles calculations based on density functional theory were used to study the red to yellow phase transformation.

Introduction

There is a continuing interest in the photophysical and chemical properties of Pt^{II} complexes. The electronic structure of square-planar Pt^{II} systems can be easily modified by ligand variation. Moreover, crystal packing has a strong effect on the nature of the lowest electronic states of these d^8 systems.[1] Optical spectroscopic studies are a particularly valuable technique for investigation of excited-state structures.[2] The anisotropic properties of the Pt^{II} complexes in some solid-state structures indicate that stacking interactions can be used to tune the spectroscopic properties.[3–5]

Polymorphism in crystalline Pt(diimine) complexes is rather common. One example is $Pt(bpy)Cl_2$ (bpy = 2,2′-bipyridine), which has two types of stable crystal structures at room temperature:[5] a yellow form containing (more or less) isolated $Pt(bpy)Cl_2$ units and a red form in which there is Pt···Pt stacking. As a result, the electronic structures and, as a consequence, the optical spectroscopic properties are different in the two cases. Miskowski et al. as well as Gray et al. have found that the origin of the emissions from the yellow and red form are completely different even though the maximum of the emission bands are roughly the same at room temperature.[1,6] In the weakly luminescent yellow form, the Pt^{II} complexes are spatially well separated from each other (the Pt–Pt distance is 4.44 Å), but in the strongly emitting red form the square-planar $Pt(bpy)Cl_2$ units stack to form an approximately linear Pt–Pt chain with a metal–metal spacing of 3.45 Å.[7] Previous investigations on Pt^{II} linear-chain systems have shown that their electronic absorption and luminescence properties strongly depend on the intra-chain metal–metal separation.[4] Thus, modifications of the Pt–Pt distance induced by decreasing from room temperature (RT) to 20 K give rise to shifts of the luminescence band maximum of about 970 cm^{-1} corresponding to an estimated reduction of the Pt–Pt distance by 0.08 Å.[7] However, the contribution of intrinsic and extrinsic temperature contributions to the emission band can be tricky to distinguish. The application of high pressure represents an extraordinary tool[2,8] that allows us to reduce the Pt–Pt distance in a continuous way. In this paper we will correlate the crystal and electronic structures by means of absorption and emission spectroscopy as well as density functional theory (DFT) calculations.

[a] Dept. de Física Aplicada, Facultad de Ciencias, Universidad de Cantabria,
Avda. de Los Castros s/n, 39005 Santander, Spain
Fax: +34-942-201402
E-mail: rafael.valiente@unican.es
[b] Dept. de Física de Materiales, Facultad de Químicas, Univ. del Pais Vasco,
20018 San Sebastián, Spain
[c] Institute for Theoretical Chemistry, Chemistry and Biochemistry Department, The University of Texas at Austin,
Texas 78712-0165, USA
[d] Dept. de Física Aplicada I, E.T.S. Ingenieros Industriales y Telecomunicaciones, Universidad del País Vasco,
48013 Bilbao, Spain
[e] Dept. of Inorganic, Analytical and Applied Chemistry, Faculty of Science, University of Geneva,
1211 Geneva, Switzerland

Results and Discussion

In Figure 1 the RT luminescence spectra of $Pt(bpy)Cl_2$ at ambient pressure, 4.7, 12.1, 17.7, and 38.0 kbar (from bottom to top) after excitation at 22260 cm^{-1} are shown. Within the square-planar symmetry the ambient-pressure luminescence band is assigned to the $\pi^*(bpy) \rightarrow d\sigma^*(Pt)$

luminescence transition (Figure 1).[7] The excitation spectrum at 16535 cm^{-1} under the same conditions has also been obtained. The low-energy band responsible for the absorption edge was assigned to the $d\sigma^*(Pt) \rightarrow \pi^*$ (bpy) transition.[9] The required small crystal size precluded the measurement of a high-quality optical absorption spectrum even under ambient-pressure conditions.

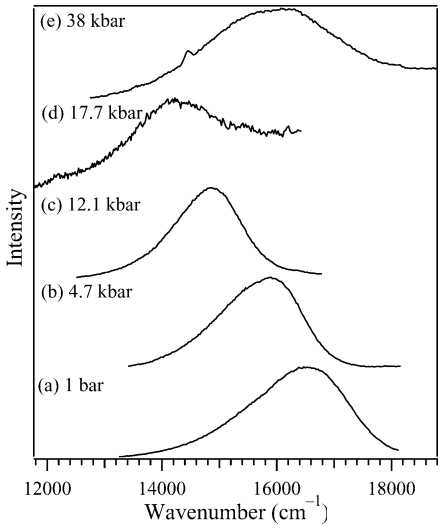

Figure 1. Room-temperature pressure dependence of the luminescence spectra of the red form of $Pt(bpy)Cl_2$.

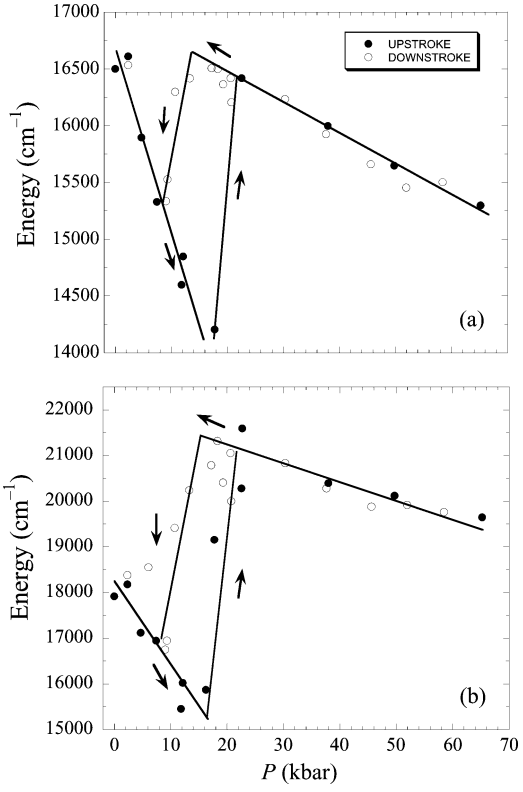

Figure 2. (a) Energy of the luminescence band maximum of the red form as a function of pressure; full circles correspond to increasing-pressure experiments and open circles to release-pressure experiments. (b) Energy of the excitation edge of the red form as a function of pressure; full circles correspond to increasing-pressure experiments and open circles to release-pressure experiments.

Figure 2 displays the pressure dependence of the emission-band maximum (a) as well as the absorption-edge energy in the excitation spectra (b) at RT. A shift to lower energies of the emission-band maximum and absorption edge is observed upon increasing the pressure from 1 bar to 17.7 kbar. At pressures higher than 17.7 kbar an abrupt blueshift is detected. Above this pressure a significant luminescence intensity decrease is observed. Moreover, the emission band broadens and the shape of the excitation spectrum alters. A change of the crystal color from orange to yellowish is observable when applying pressures larger than 17.7 kbar. Up to this pressure, the emission shift rate is –147 $cm^{-1}\,kbar^{-1}$. A similar pressure-dependent redshift of –99 $cm^{-1}\,kbar^{-1}$ was observed for crystalline $[Pt(SCN)_2\{\mu\text{-}(SCN)Mn(NCS)(bipy)_2\}_2]$.[10] Above 20 kbar the energy-band maximum is redshifted with a rate of –27 $cm^{-1}\,kbar^{-1}$ (Figure 2a). The solid lines are linear regression fits to the experimental data. Similar pressure behavior is observed for the absorption-edge energy in the excitation spectra (Figure 2b).

Crystal and Electronic Structures of the Red and Yellow Forms at Ambient Pressure

The red form of $Pt(bpy)Cl_2$ crystallizes in the *Cmcm* orthorhombic space group where the units exhibit a parallel linear chain structure along the *c* axis.[7] The space between adjacent complexes within the chain is 3.45 Å. To avoid ligand interaction the neighboring complexes are alternatively rotated by 180° within the chain (Figure 3). Moreover, the Pt^{II} atoms are somewhat displaced with respect to the *c* axis in a slight zigzag structure (ca. 161°). Angles and distances within the $Pt(bpy)Cl_2$ complex in the red form are similar to those in the yellow form, indicating that interaction between complexes in the red form does not perturb the molecular structure (Figure 4). In the yellow form, the distance between Pt^{II} nearest neighbors is 4.44 Å.[11] In Table 1 we compare the experimental angles and distances in the yellow and red forms with those obtained after geometric optimization calculations. The large Pt–Pt distance in the yellow form clearly indicates the absence of any metal–metal interactions, allowing us to consider the molecular units as isolated monomers.

The symmetry of the $Pt(bpy)Cl_2$ complex is C_{2v}. A molecular orbital diagram of an isolated complex of this type is shown in Figure 5a. The interaction between complexes along the *z*-axis induces substantial changes in the electronic structure (see Figure 5). Within a dimer model, the d_{z^2} orbital is strongly destabilized. The overlap of the d_{z^2} orbitals of adjacent Pt^{II} atoms leads to bonding $d\sigma$ and antibonding $d\sigma^*$ orbitals both of which are fully occupied (Figure 5b).[1]

Below a critical Pt–Pt distance, the highest occupied molecular orbital (HOMO) is $d\sigma^*$. Thus, the room-temperature luminescence of the red form of $Pt(bpy)Cl_2$ originates

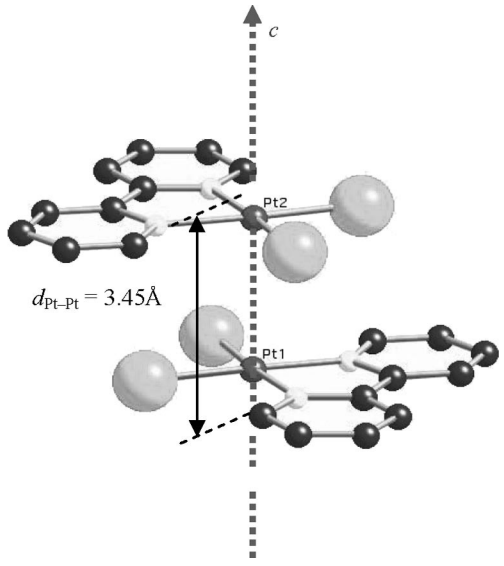

Figure 3. Perspective drawing of the dimer structure of Pt(bpy)Cl_2.

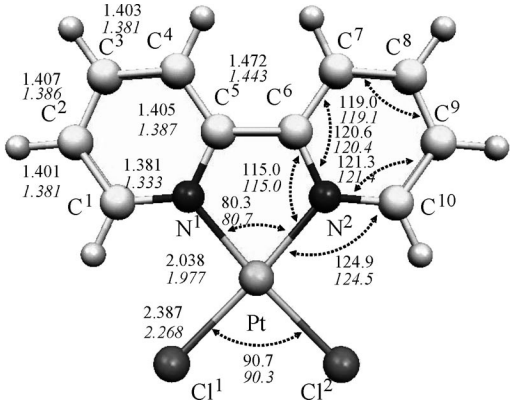

Figure 4. Geometry of the Pt(bpy)Cl_2 monomer as obtained through B3LYP/lanl2dz (top numbers) and LDA/tzp (bottom, italic numbers). Distances are given in Å and angles in °.

Table 1. Comparison between the available experimental geometry information on the yellow and red forms of Pt(bpy)Cl_2 and the calculations presented in this paper. Distances are given in Å and angles in °.

Parameter	Monomer B3LYP	Monomer BLYP	Monomer LDA	Yellow form[28]	Red form[27]
Pt–Cl	2.387	2.347	2.268	2.281–2.300	2.306
Pt–N	2.038	2.050	1.977	2.006–2.011	2.001
C^5–C^6	1.472	1.469	1.443	1.462	1.51
Cl^1–Pt–Cl^2	90.7	90.2	90.3	89.1	88
Cl^1–Pt–N^1	94.5	95.1	94.5	94.3–96	96
Cl^2–Pt–N^1	174.8	174.7	175.2	174.7–175.9	184
N^1–Pt–N^2	80.3	79.6	80.7	–	80

from a ^{3}MLCT state and is associated with the π*(bpy) → dσ*(Pt) charge-transfer transition, i.e. the LUMO π* orbital is mainly centered on the bipyridine ligand. This is in contrast to the tetracyanidoplatinates, where the luminescence is due to a pσ*(Pt) → dσ*(Pt) transition.[12]

Under ambient-pressure conditions the luminescence of the red form of Pt(bpy)Cl_2 consists of an asymmetric band

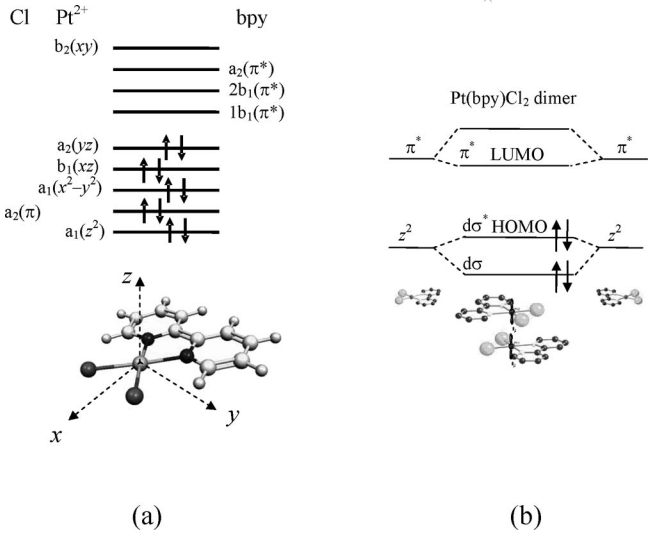

Figure 5. (a) Diagram of the frontier orbitals of the Pt(bpy)Cl_2 monomer and scheme showing the axis set chosen in the calculation. (b) Simplified energy-level scheme for the dimer model of Pt(bpy)Cl_2.

at 16535 cm^{-1} associated with the π*(bpy) → dσ*(Pt) transition (Figure 1). The excitation spectrum of the 16535 cm^{-1} luminescence is characterized by an excitation edge and a set of overlapping bands. It is similar to the polarized absorption spectrum of the red form of Pt(bpy)Cl_2 with $\mathbf{E}\perp\mathbf{c}$.[9] The temperature dependence of the emission spectrum of the red form showed a shift to lower energies. The observed behavior is due to the reduction of the Pt–Pt distance within the chain, which induces an increase in the splitting between dσ and dσ* orbitals and a reduction of the HOMO–LUMO energy gap. Gray et al. carried out temperature-dependent X-ray diffraction and luminescence experiments on the red form of Pt(bpy)Cl_2.[7] With decreasing temperature, the compound contracts anisotropically, the Pt–Pt separation decreases to 3.37 Å at 20 K, and this is accompanied by a –970 cm^{-1} redshift of the emission-band maximum. This result reveals the following relation between the luminescence maximum ν_{max} and the Pt–Pt distance R (ν_{max} and R are in units of cm^{-1} and Å, respectively) [Equation (1)].[7]

$$\nu_{max} = 29500 - 5.4\times10^5 R^{-3} \quad (1)$$

Considering that the implicit temperature term is negligible, it is possible to use this equation to calculate the pressure-dependent distance reduction.

High-Pressure Measurements and DFT Calculations

Recently, we have explored the role of the intermolecular stacking interaction by tuning the spectroscopic properties of the linear Pt–Pt chains as a function of hydrostatic pressure.[13] In view of the lack of experimental high-pressure crystal structures, we assume the validity of Equation (1) for evaluating the Pt–Pt distance reduction upon pressure in the red form. Under this assumption we estimate that the

Pt–Pt distance decreases from 3.46 Å at ambient pressure to 3.25 Å at 17.7 kbar. Our calculations suggest that pressure destabilizes the dσ* HOMO, but the bpy π* LUMO energy is only weakly pressure-dependent (Figure 6). Experimentally, as pressure is increased above 17.7 kbar, abrupt blue-shifts of 2500 cm^{-1} and 2880 cm^{-1} in the luminescence and excitation spectra (Figures 1 and 2) are observed. Our results indicated that this phase transition is likely due to the conversion of the red modification of $Pt(bpy)Cl_2$ to a high-pressure denser yellow form (HPYF), not necessarily the same yellow form observed at ambient pressure (APYF). There is no crystallographic data available for this new yellow form. Phase transitions induced by pressure have been reported previously for several $Pt(CN)_4^{2-}$ systems.[4] Some tetracyanidoplatinates exhibit similarly strong emission discontinuities due to first-order phase transitions that occur upon cooling to cryogenic temperatures.[4] Red $Pt(bpy)Cl_2$ does not undergo any phase transition even when cooled to 20 K.[7] Since the emission intensity of the APYF is much weaker than that of the red form, it has been proposed that APYF is a ^{3}LF emitter.[6] The same argument could reasonably be applied for the HPYF, whose emission is also much weaker than that of the red form. Because of the similarity of the HPYF and APYF emissions and the densities of the red form and the APYF (2.56 and 2.65 $g\,cm^{-3}$, respectively), it could be thought that HPYF and APYF are the same phase. The emission maxima of Pt^{II} ^{3}LF states exhibit comparatively weak pressure dependences, with typical shift rates in the order of 10–40 $cm^{-1}\,kbar^{-1}$.[14] From our system, we find a shift rate of $d\nu_{max}/dP = -27\ cm^{-1}\,kbar^{-1}$ (Figure 2a), and a high-pressure emission bandwidth (FWHM) of 3065 cm^{-1}, close to the value of 4030 cm^{-1} found for the emission bandwidth in yellow $Pt(bpy)Cl_2$ at 250 K at ambient pressure.[6] A somewhat narrower luminescence bandwidth at elevated pressures is to be expected, owing to diminished relative distortions of the emissive and ground states.[2,15] The same effect accounts for the narrower bandwidth associated with the 12 kbar luminescence of red $Pt(bpy)Cl_2$ (Figure 1c) relative to that observed in the ambient-pressure spectrum (Figure 1a). Finally, the order-of-magnitude decrease in luminescence intensity accompanying the phase transition at 17.7 kbar is also consistent with a change from red to yellow $Pt(bpy)Cl_2$, i.e. a change from charge transfer to ligand-field luminescence transitions. The room-temperature ambient pressure luminescence quantum yields of microcrystalline samples of these two compounds are known to differ by more than an order of magnitude.[5] Pressure-dependent excitation spectra confirm our interpretation of the crystallographic phase transition at 17.7 kbar: between 12 and 23 kbar the absorption edge shifts discontinuously from 15000 to 20325 cm^{-1} (Figure 2b).

The character and reversibility of the phase transition was highlighted by the luminescence spectra as well as the excitation spectra recorded upon increasing and releasing pressure. Figure 2 shows that upon pressure release, the yellow-to-red phase transformation only occurs at 11.0 kbar. Therefore, there is a hysteresis in the luminescence properties of $Pt(bpy)Cl_2$ of about 8 kbar. The presence of this hysteresis indicates that HPYF and APYF are different phases. In the 11.0–17.7 kbar range, depending on the pressure history, the luminescence originates in the ^{3}MLCT or in the ^{3}LF state.

In our calculations, the long Pt–Pt distance and the similarities in geometry between the $Pt(bpy)Cl_2$ monomer units in the two modifications allow us to simulate the yellow form using a single in-vacuo monomer, while the red form is obtained by stacking two (dimer) or three (trimer) $Pt(bpy)Cl_2$ units. In this model, the effect of applying hydrostatic pressure is simulated by varying the Pt–Pt distance R.

The monomer geometry was first optimized at the B3LYP/lanl2dz level imposing C_{2v} symmetry. The result of this calculation is summarized in Figure 4 (plain numbers), and a comparison with available experimental data[11] is shown in Table 1. The agreement between them is very good

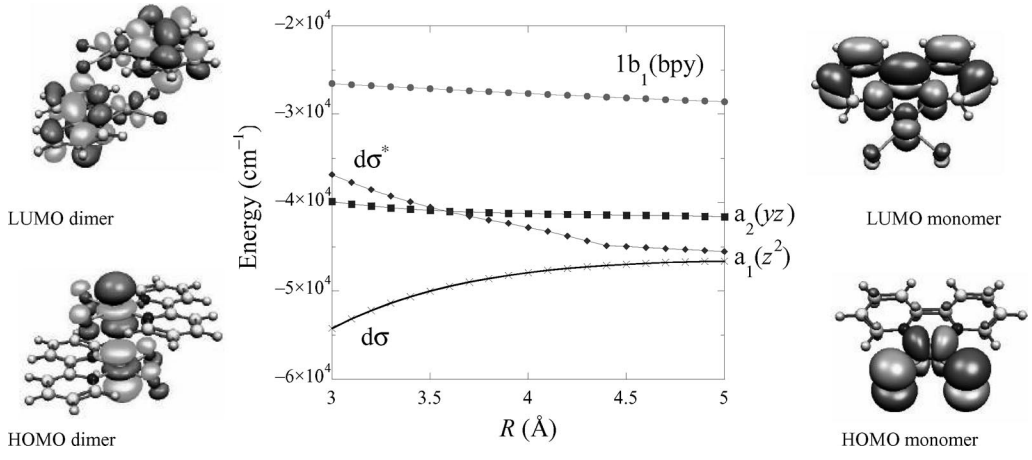

Figure 6. Variation of selected orbital energies of the $Pt(bpy)Cl_2$ dimer with the interlayer distance. Labels corresponding to the orbitals in the yellow and red form are shown on the right and left part of the plot, respectively. The antibonding dσ* orbital becomes the HOMO for R values smaller than 3.6 Å after crossing with $a_2(yz)$, which corresponds to the HOMO in the monomer (yellow phase), reducing the HOMO–LUMO gap as R is decreased.

with the exception of the Pt–Cl distance which is 0.08 Å longer in the calculations. A second optimization was carried out at the LDA/tzp level (italic numbers in Figure 4). In this case the Pt–Cl distance is in better agreement with experimental findings (see Table 1). In order to find the source of this error in the calculation we performed an LDA/lan2dz optimization that resulted in an overestimation of the Pt–Cl distance. Thus, we conclude that the longer distances found in these calculations are due to the basis set, possibly because the core–core interactions between the pseudopotentials found in the lanl2dz basis set are overestimated. This argument is supported by a BLYP/tzp level calculation (with exactly the same basis set as LDA/tzp). This resulted in a monomer geometry (Table 1) that is very close to the one calculated with LDA/tzp. As the agreement between the LDA/tzp geometries with those of the experiments is good (see Table 1), we use this geometry throughout this section to represent the monomer.

The symmetry, spacing, and character of the most important orbitals of Pt(bpy)Cl_2 as calculated in LDA are shown in Table 2 and Figure 5a, similar results were found when using B3LYP and BLYP.

Table 2. Energy and character of the most important orbitals of the Pt(bpy)Cl_2 monomer as obtained in LDA/tzp.

Orbital	Energy [cm^{-1}]	Orbital character [%] Pt	Cl	bpy
	Unoccupied			
$b_2(xy)$	20810	46	34	20
a_2	20485	2	0	98
$2b_1$	18550	2	0	98
$1b_1$	12420	4	0	96
	Occupied			
$a_2(yz)$	0	27	70	3
$b_1(xz)$	–1050	31	64	5
$a_1(x^2–y^2)$	–2660	34	65	1
b_2	–3950	2	95	3
$a_1(z^2)$	–4030	84	12	4

According to Figure 5 and Table 2, the three occupied orbitals with highest energy, $a_2(yz)$, $b_1(xz)$, and $a_1(x^2–y^2)$, have a strong $Cl(p_\pi)$ character with very significant Pt(d) hybridization. The electrons in the lowest frontier orbital, $a_1(z^2)$, lie almost completely on the Pt ion and are perpendicular to the plane of the molecule. The LUMO and the next two orbitals above it are localized on the bpy ligand and have a strong π* character. The first unoccupied orbital mainly belonging to the $PtCl_2$ unit is $b_2(xy)$ which lies 20810 cm^{-1} above the HOMO. These findings are similar to those reported for Pt(bpym)Cl_2.[16]

We have used the TD-B3LYP/lanl2dz method to calculate the low-lying excited states of the monomer. They are presented in Table 3 along with the estimation of the same transition energies by the ΔSCF method in LDA and BLYP. The reliability of these results is supported by the close agreement between the three different calculation methods. The energy of the most intense singlet-singlet transition, 21615 cm^{-1}, compares well with the position of the first peak in the absorption spectrum of the yellow form[17] lying at ca. 21000 cm^{-1}. This transition does not correspond to the HOMO–LUMO one, but it also has a strong dπ → π* character. The second most intense peak, $b_1(xz) \rightarrow 2b_1(\pi^*)$, $a_2(yz) \rightarrow a_2(\pi^*)$, is located at energies where the experimental spectrum presents another band. The emission spectrum of the yellow form is almost undetectable at RT.[5] For this reason and based on semiempirical extended Hückel calculations,[18] Miskowski et al.[19] proposed that the emission in the yellow form is due to a d-d ^{3}LF transition.[6] In order to check this hypothesis we have performed a geometry optimization for the $^1B_1$ state [with the promoted electron in the $b_2(xy)$ orbital] and for the $^1B_2$ and $^1A_1$ states [with the promoted electron in the π*(bpy) orbital]. Results of these calculations are presented in Table 4. In the $^1B_1$ state the Pt–ligand distances increase very significantly with respect to those in the ground state: about 0.20 Å for Pt–N and 0.06 Å for Pt–Cl (Table 4). The ligand–Pt–ligand angles also change strongly. This fact leads to a large Stokes shift: the absorption $d\pi(Pt) \rightarrow b_2(xy)$ is at 22985 cm^{-1}, and the emission $b_2(xy) \rightarrow d\pi(Pt)$ is at 18145 cm^{-1} (in the LDA calculations). In the case of $^1B_2$ and $^1A_1$ states, Pt–ligand distances and ligand–Pt–ligand angles hardly vary with respect to the ground state. However, an important reorganization takes place within bpy: the two pyridine rings approach each other; i.e. the C^5–C^6 distance is reduced by 5 pm. In the case of the $^1B_2$ excited state, this change in the bpy ligand produces an important Stokes shift, from 15890 cm^{-1} in absorption to 14680 cm^{-1} in emission. Since the calculated energy of the relaxed $^1B_2$ state is lower than the energy of $^1B_1$, in-vacuo single molecule DFT calculations predict that emission occurs from the first ($^1B_2$) state, in contrast to the experimental assignment by Miskowski et al. (in solution). In principle, the π*(bpy) → dπ(Pt) transition should have an emission intensity of the same order of magnitude as in the red form, because both seem to be predominantly ^{3}MLCT. However, our theoretical calculations suggested that dπ(Pt) orbitals have a larger Cl(2p) character than Pt(d) ones (Table 1). In conclusion, the emission transition experimentally attributed to a π*(bpy) → dπ(Pt) transition[6] is likely to have mixed metal-to-ligand charge-transfer character with an important halide–ligand contribution.[16] This may well be the reason for its low intensity when compared to the red form where the HOMO is mostly a Pt(z^2) orbital. Other experimental findings, like the lack of vibronic structure and large bandwidths, are also consistent with the variation of geometry of the $^1B_2$ excited state when compared to the ground state and provide further support for the assignment given here. A similar conclusion to the one reached here was presented in ref.[16] where this transition was assigned to a halide-to-ligand charge-transfer (XLCT). In that work the effect of solvents in the simulation was also checked, and it was found that the calculations reproduced well the experimental trends.

In the red form, the overlap between the z^2 orbitals on adjacent Pt atoms destabilized the dσ* dimer level. According to our calculations, the emission in the red form unambiguously comes from the π*(bpy) → σ*(z^2, Pt) transition

Table 3. Description of some selected excited states of the Pt(bpy)-Cl_2 monomer as calculated by TD-B3LYP. Comparison with the energies obtained in LDA and BLYP by the ΔSCF method and absorption experiment. All energies are given in cm^{-1}.

State	Main character	TD-B3LYP/lanl2dz		BLYP	LDA	Exp.[17]
		ΔE	Osc. str.	ΔE	ΔE	
$^1B_2$	$a_2(yz) \rightarrow 1b_1$(bpy)	17340	0.0004	16370	17100	ca. 19030
$^1A_1$	$b_1(xz) \rightarrow 1b_1$(bpy)	21615	0.0057	17825	18790	ca. 20970
$^1A_1$	$b_1(xz) \rightarrow 2b_1$(bpy) $a_2(yz) \rightarrow a_2$(bpy)	26695	0.0017	25245	26290	ca. 25000
$^1B_1$	$a_2(yz) \rightarrow b_2(xy)$	28790	0.0000	22015	27100	–

(Figure 5b), which has a clear ^{3}MLCT nature, and therefore is very intense (see below).

We have simulated the red form of $Pt(bpy)Cl_2$ by stacking two and three monomers on top of each other. As in the case of the monomer, the LUMO in these molecules has bpy(π*) character (Figure 6). However, the HOMO is strongly localized on the Pt atom and has z^2 character. Calculating the HOMO–LUMO transition for the dimer and trimer using the experimental separation between Pt ions leads to 18630 and 15240 cm^{-1} energy gaps. A similar behavior is observed in experiments where the red-form emission energy is lowered when pressure is applied.

In order to understand the changes between the dimer (red phase) and the monomer (yellow phase) we have plotted in Figure 6 the energies of some selected orbitals of the dimer as a function of interlayer distance R. The energies of the monomer HOMO, $a_2(xy)$, and LUMO are quite insensitive to the application of pressure. Moreover, the LUMO is the same for the monomer and the dimer. However, the energy of the dimer orbitals, which at long distance become the monomer $a_1(z^2)$ ones, are strongly split in a bonding (dσ) and antibonding pair (dσ*) when R is reduced. A reduction of the Pt–Pt distance increases the z^2 interaction destabilizing the dσ* dimer level. In fact, the dσ* orbital becomes the HOMO for R values smaller than 3.6 Å, i.e. dσ* must be the HOMO in the red form. From that point onwards the Pt–Pt distance decrease is accompanied by a continuous reduction of the HOMO–LUMO gap that explains the shift of the emission to lower energies of the red form when compared with the yellow one. We have calculated the rate at which the HOMO–LUMO transition energy in the dimer changes when R is varied around R = 3.45 Å by the ΔSCF method and obtained dE_{H-L}/dR = 7900 cm^{-1} $Å^{-1}$. Taking into account the value of the experimental linear compressibility, $\chi_c = 3.4 \times 10^{-3}$ $kbar^{-1}$,[13] we estimate a redshift of –93 cm^{-1} $kbar^{-1}$ for the emission upon pressure. This value compares reasonably well with the experimental value of –147 cm^{-1} $kbar^{-1}$ considering the limitations of our models. Because the arrangement of the monomers in HPYF is unknown, it has not been possible to study the pressure dependence of the luminescence for this phase.

In Figure 7 the variation of the total energy of the dimer and trimer with the Pt–Pt separation in LDA calculation is represented. In the dimer, this curve presents a minimum at R = 3.28 Å, which is reasonably close to the experimental R_0 value of 3.45 Å. When three instead of two $Pt(bpy)Cl_2$ units are used, the optimum interlayer separation is slightly shifted to 3.38 Å, significantly closer to the experimental value. From Figure 7 we learn that the inter-monomer potential is very anharmonic indicating that if the dimer is compressed enough, electrostatic repulsion becomes the dominant effect and a geometry with two independent, noninteracting $Pt(bpy)Cl_2$ molecules will be favored.

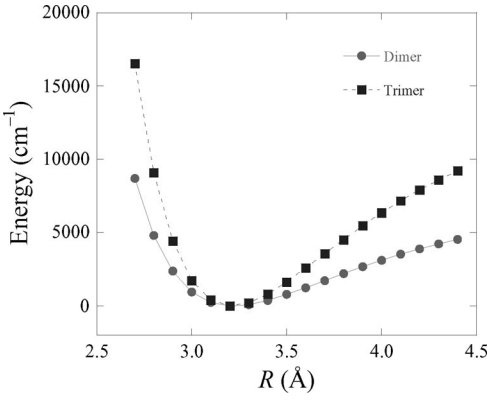

Figure 7. Total energy of the ground state of the $Pt(bpy)Cl_2$ dimer (circles) and trimer (squares) at the LDA/tzp level when the interlayer distance is varied.

Table 4. Description of the changes in the geometry of $^1A_1$, $^1B_2$, and $^1B_1$ with respect to the ground state for the same parameters as in Table 1. Positive values indicate an increase of the distances or angles with respect to the ground state. Distances are given in Å and angles in °. Energies obtained in LDA and BLYP calculations by the ΔSCF method for the emission and the corresponding Stokes shift are also shown. All energies are given in cm^{-1}.

Parameter	$^1A_1[1b_1(bpy) \rightarrow b_1(xz)]$		$^1B_2[1b_1(bpy) \rightarrow a_2(yz)]$		$^1B_1[b_2(x^2–y^2) \rightarrow a_2(yz)]$	
	Monomer BLYP	Monomer LDA	Monomer BLYP	Monomer LDA	Monomer BLYP	Monomer LDA
Pt–Cl	–0.005	–0.003	–0.012	–0.012	0.069	0.063
Pt–N	–0.002	0.004	–0.006	0.002	0.227	0.180
C^5–C^6	–0.042	–0.035	–0.059	–0.049	0.016	0.014
Cl^1–Pt–Cl^2	–1.9	–1.9	–0.5	–0.6	8.7	7.0
Cl^1–Pt–N^1	0.5	0.4	–0.3	–0.2	–0.7	–0.5
Cl^2–Pt–N^1	1.5	1.5	0.8	0.8	–8.0	–6.5
N^1–Pt–N^2	1.0	1.1	1.1	1.0	–7.3	–6.0
Emission	16050	17180	13630	14680	12740	18145
Absorption	16935	17985	15000	15890	17660	22985
Stokes shift	885	805	1370	1210	4920	4840

Conclusions

We present a theoretical interpretation of the red-to-yellow phase transition experimentally observed in $Pt(bpy)Cl_2$ microcrystals at high pressures. Our theoretical models are based on isolated $Pt(bpy)Cl_2$ units (to simulate the yellow form) and dimer and trimer units of this complex to simulate the stacked, linear-chain red form. DFT calculations allow us to analyze the differences between red and yellow phases observed experimentally in terms of the Pt–Pt distance. The appearance of hysteresis in the optical properties most probably indicates that the new yellow phase observed at high pressure and the ambient-pressure yellow phase are distinct phases. The calculations suggest that the high-pressure luminescence corresponding to the high-pressure yellow phase is a halide–ligand transition instead of a ligand-field transition. This is a clear example where a synergy between experimental and theoretical work is essential for understanding high-pressure effects.

Experimental Section and Computational Details

Synthetic Procedure: $Pt(bpy)Cl_2$ samples of the yellow form were prepared as described in refs.[13,17,20]

Spectroscopic Measurements: Hydrostatic-pressure experiments were carried out in a diamond-anvil cell (High Pressure Diamond Optics, Inc.) using spectroscopic paraffin as the pressure-transmitting medium. Excitation and luminescence spectra were performed with a Jobin–Yvon FluoroMax-2 fluorometer with a microscope attached. An optic fiber guided the emission light to the fluorometer detection system. All the spectra were corrected for instrumental response. A pre-indented aluminum gasket with a 300-μm diameter hole (machined with a Natjet microdrill) was used. The applied pressure was measured through the redshift luminescence of the ruby R-lines. Ruby luminescence was excited with the 407 nm line of a Kr^+ laser (Coherent CR-500K) and dispersed by a Jobin–Yvon U1000 double-monochromator.

DFT Studies: The geometry of the electronic ground state of a single $Pt(bpy)Cl_2$ unit has been obtained using DFT calculations through the semiempirical hybrid functional B3LYP[21,22] and the LANL2DZ basis set which includes pseudopotentials to represent the core electrons. Time-dependent DFT (TDDFT) was later used to explore the position and character of several excited states at this level of theory. All these calculations were constrained to keep C_{2v} symmetry. The Gaussian 98[23] program suite was employed. As a complement to the previous calculations the geometry of a $Pt(bpy)Cl_2$ molecule and the electronic structure of the monomer, dimer, and trimer for different values of the Pt–Pt distance and Pt–Pt–Pt angle were also calculated using the ADF package.[24] Two types of calculations were performed: (a) Using the local density approximation (LDA) within the VWN parameterization of the electron correlation[25] and (b) using the generalized gradient approximation (GGA) exchange-correlation through the Becke[21] functional for exchange and Lee–Yang–Parr[26] functional for correlation (BLYP). In both cases relativistic effects have been taken into account through the Zeroth-Order Regular Approximation (ZORA),[27] which includes the Darwin and mass-velocity terms, but not the spin-orbit interaction. All atoms were described through basis sets of TZP quality (triple-ζ STO plus-one polarization function) given in the program data base and taking into account all electrons (without any frozen-core or pseudopotential approximations). Electronic transition calculations at this level of theory were performed with the ΔSCF method. In the case of absorption spectra the ΔSCF method consists of a geometry optimization for the ground state, yielding the corresponding E_1 energy. At the same geometry the electronic configuration of an excited state is imposed, and the SCF procedure is performed again, to obtain the corresponding E_2 energy. The energy difference, $E_2 - E_1$, is taken as the electronic transition energy. For the emission spectra the procedure is similar, but in this case the geometry optimization is performed imposing the electronic configuration of the excited state, and the energy of the ground state is then calculated at that geometry.

Acknowledgments

This work was financially supported by the Spanish Ministerio de Educación y Ciencia under project no. MAT2005-00099. O. S. W. acknowledges funding from the Swiss National Science Foundation.

[1] W. B. Connick, V. M. Miskowski, V. H. Houlding, H. B. Gray, *Inorg. Chem.* **2000**, *39*, 2585–2592.
[2] O. S. Wenger, R. Valiente, H. U. Güdel, *J. Chem. Phys.* **2001**, *115*, 3819–3826.
[3] M. Kato, A. Omura, A. Toshikawa, S. Kishi, Y. Sugimoto, *Angew. Chem. Int. Ed.* **2002**, *41*, 3183–3185.
[4] G. Gliemann, H. Yersin, *Struct. Bonding (Berlin)* **1985**, *62*, 87–153.
[5] V. H. Houlding, V. M. Miskowski, *Coord. Chem. Rev.* **1991**, *111*, 145–152.
[6] V. M. Miskowski, V. H. Houlding, C. Che, Y. Wang, *Inorg. Chem.* **1993**, *32*, 2518–2524.
[7] W. B. Connick, L. M. Henling, R. E. Marsh, H. B. Gray, *Inorg. Chem.* **1996**, *35*, 6261–6265.
[8] a) C. Reber, J. K. Grey, E. Lanthier, K. A. Frantzen, *Inorg. Chem.* **2005**, *26*, 233–254; b) K. L. Bray, *Top. Curr. Chem.* **2001**, *213*, 1.
[9] M. Weiser-Wallfahrer, G. Gliemann, *Z. Naturforsch., Teil B* **1990**, *45*, 652–657.
[10] G. Levasseur-Thériault, C. Reber, C. Aronica, D. Luneau, *Inorg. Chem.* **2006**, *45*, 2379–2381.
[11] R. H. Herber, M. Croft, M. J. Coyer, B. Bilash, A. Sahiner, *Inorg. Chem.* **1994**, *33*, 2422–2426.
[12] a) H. Yersin, I. Hidvegi, G. Gliemann, *Phys. Rev. B* **1979**, *19*, 177–180; b) A. Loosli, M. Wermuth, H. U. Güdel, S. Capelli, J. Hauser, H. B. Bürgi, *Inorg. Chem.* **2000**, *39*, 2289–2293.
[13] O. S. Wenger, S. García-Revilla, H. U. Güdel, H. B. Gray, R. Valiente, *Chem. Phys. Lett.* **2004**, *384*, 190–192.
[14] M. A. Stroud, H. G. Drickamer, M. H. Zietlow, H. B. Gray, B. I. Swanson, *J. Am. Chem. Soc.* **1989**, *111*, 66–72.
[15] J. K. Grey, M. Triest, I. S. Butler, C. Reber, *J. Phys. Chem. A* **2001**, *105*, 6269–6272.
[16] W. Kaim, A. Dogan, M. Wanner, A. Klein, I. Tiritiris, T. Schleid, D. J. Stufkens, T. L. Snoeck, E. J. L. McInnes, J. Fiedler, S. Zalis, *Inorg. Chem.* **2002**, *41*, 4139.
[17] M. Textor, H. R. Oswald, *Z. Anorg. Allg. Chem.* **1974**, *407*, 244.
[18] H. H. Patterson, J. C. Tewksbury, M. Martin, M. B. Krogh-Jespersen, J. A. Lomenzo, H. O. Hooper, A. Kasi Viswanath, *Inorg. Chem.* **1981**, *20*, 2297–2301.
[19] V. M. Miskowski, V. H. Houlding, *Inorg. Chem.* **1989**, *28*, 1529–1533.
[20] G. T. Morgan, F. H. Burstall, *J. Chem. Soc.* **1934**, 965.
[21] A. D. Becke, *Phys. Rev. A* **1988**, *38*, 3098–3100.
[22] A. D. Becke, *J. Chem. Phys.* **1993**, *98*, 1372–1377.
[23] M. J. Frisch, G. W. Trucks, H. B. Schlegel, G. E. Scuseria, M. A. Robb, J. R. Cheeseman, V. G. Zakrzewski, J. A. Mont-

gomery, R. E. Stratmann, J. C. burant, S. Dapprich, J. M. Millam, A. D. Daniels, K. N. Kudin, M. C. Strain, O. Farkas, J. Tomasi, V. Barone, M. Cossi, R. Cammi, B. Mennucci, C. Pomelli, C. Adamo, S. Clifford, J. Ochterski, G. A. Petersson, P. Y. Ayala, Q. Cui, K. Morokuma, D. K. Malick, A. D. Rabuck, K. Raghavachari, J. B. Foresman, J. Cioslowski, J. V. Ortiz, B. B. Stefanov, G. Liu, A. Liashenko, P. Piskorz, I. Komaromi, R. Gomperts, R. L. Martin, D. J. Fox, T. Keith, M. A. Al-Laham, C. Y. Peng, A. Nanayakkara, C. Gonzalez, M. Challacombe, P. M. W. Gill, B. G. Johnson, W. Chen, M. W. Wong, J. L. Andres, M. Head-Gordon, E. S. Replogle, J. A. Pople *Gaussian 98*, Gaussian Inc., Pittsburgh, PA, **1998**.

[24] a) S. J. A. van Gisbergen, J. G. Snijders, E. J. Baerends, *Comput. Phys. Commun.* **1999**, *118*, 119–138; b) G. te Velde, F. M. Bickelhaupt, S. J. A. van Gisbergen, C. Fonseca Guerra, E. J. Baerends, J. G. Snijders, T. Ziegler, *J. Comput. Chem.* **2001**, *22*, 931–967.

[25] S. H. Vosko, L. Wilk, M. Nusair, *Can. J. Phys.* **1980**, *58*, 1200–1211.

[26] C. Lee, W. Yang, R. G. Parr, *Phys. Rev. B* **1988**, *37*, 785–789.

[27] E. van Lenthe, E. J. Baerends, J. G. Snijders, *J. Chem. Phys.* **1994**, *11*, 9783.

[28] R. S. Osborn, D. Rogers, *J. Chem. Soc. Dalton Trans.* **1974**, *9*, 1002–1004.

Received: January 17, 2007
Final Revision Received: September 28, 2007
Published Online: November 13, 2007

